i An update to this article is included at the end

International Journal of Solids and Structures 110–111 (2017) 294–304

Contents lists available at ScienceDirect

International Journal of Solids and Structures

journal homepage: www.elsevier.com/locate/ijsolstr

Shear wave propagation in finitely deformed 3D fiber-reinforced composites

Pavel I. Galich, Viacheslav Slesarenko, Stephan Rudykh*

Department of Aerospace Engineering, Technion – Israel Institute of Technology, Haifa 32000, Israel

ARTICLE INFO

Article history:
Received 19 September 2016
Revised 19 November 2016
Available online 13 December 2016

Keywords:
Fiber-reinforced composites
Wave propagation
Finite deformations
Dispersion
Transversely isotropic
Micromechanics

ABSTRACT

We investigate the propagation of shear waves in finitely deformed 3D fiber-reinforced composites. We employ a micromechanics based approach and derive explicit expressions for the phase and group velocities of the shear waves in the long wave limit. Thus, we obtain the important characteristics of the shear waves in terms of the volume fractions and material properties of the constituents. We find that the phase and group velocities significantly depend on the applied deformation and direction of wave propagation. To account for interactions between the elastic waves and microstructure in finitely deformed 3D periodic fiber-reinforced materials, we employ the Bloch wave analysis superimposed on large macroscopically applied homogeneous deformations, and we implement the technique into a finite element code. The Bloch wave numerical analysis reveals the essential dispersion phenomenon for the shear waves propagating along the fibers in the finitely deformed 3D periodic fiber-reinforced materials. We find that the appearance of the dispersion phenomenon and the corresponding wavelengths can be tuned by material composition and deformation.

© 2016 Elsevier Ltd. All rights reserved.

1. Introduction

Nature actively exploits sophisticated microstructures to achieve remarkable material properties and functionalities. In particular, the fiber-reinforced deformable composites, possessing a light weight, high strength and flexibility at the same time, are widely present in nature (Saheb and Jog, 1999). However, natural materials are biodegradable and poorly resistant to moisture, and not always they can provide desirable properties; therefore, synthetic composite materials are of a great interest. The mechanical performance of composite materials can be tailored by designing microstructures combining soft and stiff constituents. Recent advances in the material fabrication techniques and 3D-printing already allow realization of microstructured metamaterials with various properties and functionalities (Babaee et al., 2013; Kolle et al., 2013; Rudykh and Boyce, 2014a; Lin et al., 2014; Ge et al., 2013; Bafekrpour et al., 2014; Rudykh et al., 2015; Celli and Gonella, 2015; Srivastava, 2016; Golub et al., 2012; Fomenko et al., 2014). Moreover, *soft* metamaterials can be reversibly deformed, and, thus, enabling us to manipulate their effective properties via deformation (Li et al., 2013; Slesarenko and Rudykh, 2016). Thus, for example, elastic wave propagation in soft composite materials can be controlled by deformation (Bertoldi and Boyce, 2008b; Bertoldi et al., 2008; Gei, 2008; Rudykh and Boyce, 2014b; Galich et al., 2017; Babaee et al., 2016; Chen and Elbanna, 2016). Even in relatively simple homogeneous hyperelastic materials, elastic wave characteristics can be significantly transformed via deformation (Dorfmann and Ogden, 2010; Galich and Rudykh, 2015b; 2015a; 2016). It is worth noting that many soft biological tissues are found to possess fiber-matrix microstructures (Humphrey, 2002), and the soft tissues frequently experience large deformations due to growth or other physiological processes. Hence, investigation of elastic wave propagation in 3D fiber composites (FCs) undergoing finite deformations can be beneficial for biomedical applications such as ultrasound testing.

Small amplitude elastic wave propagation in finitely deformed homogeneous isotropic materials was pioneered by Biot (1940) on the basis of the static nonlinear theory (Biot, 1939). Waves of a finite amplitude propagating in a pre-stressed elastic medium were investigated by John (1966), and Currie and Hayes (1969). Boulanger and Hayes (1992) considered wave propagation in finitely deformed incompressible Mooney–Rivlin materials and derived explicit relations for wave velocities. Boulanger et al. (1994) extended this work to a broader class of finitely deformed compressible Hadamard materials and first obtained the explicit expressions for the phase velocities of longitudinal and transversal waves. Recently, Destrade and Ogden (2013) have revised and generalized the problem of an infinitesimal wave propagation in

* Corresponding author.
E-mail address: rudykh@technion.ac.il (S. Rudykh).

http://dx.doi.org/10.1016/j.ijsolstr.2016.12.007
0020-7683/© 2016 Elsevier Ltd. All rights reserved.

the finitely deformed hyperelastic materials by application of the invariant theory. More recently, Galich and Rudykh (2015b) have investigated infinitesimal wave propagation in finitely deformed compressible Gent materials, exhibiting pronounced stiffening effects, and obtained closed form expressions for the phase velocities of longitudinal and transversal waves.

By employing the nonlinear elastic theory (Truesdell and Noll, 1965) and a phenomenological approach, Scott and Hayes (1976) considered small amplitude plane waves superimposed on a homogeneous deformation in the so-called idealized fiber-reinforced materials, assuming an incompressible matrix and inextensible fibers. Later, Scott (1991, 1992) extended this analysis and considered infinitesimal vibrations of an arbitrary form superimposed on a finite deformation for a broad class of elastic anisotropic materials. The infinitesimal elastic wave propagation in nearly incompressible and nearly inextensible fiber-reinforced materials with unidirectional and orthogonal fibers was examined by Rogerson and Scott (1994). More recently, Ogden and Singh (2011) revisited the problem of infinitesimal wave propagation in an incompressible transversely isotropic elastic solid in the presence of an initial stress. In their work, Ogden and Singh (2011) exploited the phenomenological theory of invariants and presented a more general and transparent formulation of the theory for small amplitude waves propagating in a deformed transversely isotropic hyperelastic solid.

In this work, we employ a *micromechanics* based approach accounting for the phase properties and their spatial distribution to analyze the wave propagation in finitely deformed 3D FCs, as opposite to previous works that employ phenomenological approach (Scott and Hayes, 1976; Scott, 1991, 1992; Rogerson and Scott, 1994; Ogden and Singh, 2011), or numerically model the composites in 2D settings (Rudykh and Boyce, 2014b; Bertoldi and Boyce, 2008b), or do not consider finite deformations (Aberg and Gudmundson, 1997; Kushwaha et al., 1993). Here, we derive explicit closed form expressions for phase and group velocities of the shear waves for any direction of wave propagation in finitely deformed 3D fiber-reinforced materials with neo-Hookean phases. These explicit expressions provide important information on the elastic wave propagation in the long wave limit. To account for the interaction of the elastic waves with the composite microstructure, the Bloch wave analysis is implemented in the finite element code, allowing us to analyze small amplitude motions superimposed on finite macroscopically applied homogeneous deformations. It should be noted that we analyze the finitely deformed fibrous materials in fully 3D settings – both the deformation and the direction of the wave propagation – which, to the best of our knowledge, is not covered in the existing literature. We investigate the role of the material composition and phase properties in the dispersion of shear waves. We specifically focus on the influence of deformation on the dispersion of the shear waves. By considering the waves propagating in the direction of fibers, we find that the applied deformation strongly affects the long waves; whereas the influence of the deformation is weaker for the ranges of short wavelengths. The effect of deformation is found to be more pronounced in FCs with moderate and large shear modulus contrasts between the phases and with large volume fractions of fibers. Finally, we compare the micromechanics based homogenization technique and the numerical Bloch wave analysis, thus, bringing together the different length-scale analyses, and showing the equivalence of these distinct approaches at certain ranges of wavelengths.

2. Theoretical background

Consider a continuum body and identify each point in the undeformed configuration with its vector $\mathbf{X}$. In the deformed body, the new location of the corresponding points is defined by mapping function $\mathbf{x} = \boldsymbol{\chi}(\mathbf{X}, t)$. Hence, the deformation gradient is $\mathbf{F} = \partial\mathbf{x}/\partial\mathbf{X}$, and its determinant $J \equiv \det\mathbf{F} > 0$. For a hyperelastic material described by a strain energy function $\psi(\mathbf{F})$, the first Piola–Kirchhoff stress tensor can be calculated as follows

$$\mathbf{P} = \frac{\partial\psi(\mathbf{F})}{\partial\mathbf{F}}. \tag{1}$$

For an incompressible material, $J = 1$ and Eq. (1) modifies as

$$\mathbf{P} = \frac{\partial\psi(\mathbf{F})}{\partial\mathbf{F}} - p\mathbf{F}^{-T}, \tag{2}$$

where p represents an unknown Lagrange multiplier. The corresponding Cauchy stress tensor is related to the first Piola-Kirchhoff stress tensor via the relation $\boldsymbol{\sigma} = J^{-1}\mathbf{P}\cdot\mathbf{F}^T$.

In the absence of body forces the equations of motion can be written in the undeformed configuration as

$$\mathrm{Div}\mathbf{P} = \rho_0\frac{D^2\boldsymbol{\chi}}{Dt^2}, \tag{3}$$

where ρ_0 is the initial density of the material and the operator $D^2(\bullet)/Dt^2$ represents the material time derivative. If the deformation is applied quasi-statically, the right hand part of Eq. (3) can be assumed to be zero, and the equilibrium equation is obtained as

$$\mathrm{Div}\mathbf{P} = \mathbf{0}. \tag{4}$$

Consider next infinitesimal motions superimposed on the equilibrium state. The equations of the incremental motions are

$$\mathrm{Div}\dot{\mathbf{P}} = \rho_0\frac{D^2\mathbf{u}}{Dt^2}, \tag{5}$$

where $\dot{\mathbf{P}}$ is the incremental change in the first Piola–Kirchhoff stress tensor and $\mathbf{u}$ is the incremental displacement.

The linearized constitutive law can be written as

$$\dot{P}_{ij} = \mathcal{A}_{0ijkl}\dot{F}_{kl}, \tag{6}$$

where $\dot{\mathbf{F}} = \mathrm{Grad}\,\mathbf{u}$ is the incremental change in the deformation gradient, and the tensor of elastic moduli is defined as $\mathcal{A}_{0i\alpha k\beta} = \partial^2\psi/\partial F_{i\alpha}\partial F_{k\beta}$. Under substitution of Eq. (6) into Eq. (5) the incremental motion equation takes the form

$$\mathcal{A}_{0ijkl}u_{k,lj} = \rho_0\frac{D^2u_i}{Dt^2}. \tag{7}$$

3. Long wave estimates for finitely deformed incompressible fiber composites

To analyze small amplitude motions superimposed on a finite deformation, we present equation of motion (7) in the updated Lagrangian formulation

$$\mathcal{A}_{ijkl}u_{k,lj} = \rho\frac{\partial^2u_i}{\partial t^2}, \tag{8}$$

where $\mathcal{A}_{iqkp} = J^{-1}\mathcal{A}_{0ijkl}F_{pl}F_{qj}$ and $\rho = J^{-1}\rho_0$ is the density of the deformed material.

We seek a solution for Eq. (8) in the form of plane waves with constant polarization

$$\mathbf{u} = \mathbf{g}h(\mathbf{n}\cdot\mathbf{x} - ct), \tag{9}$$

where h is a twice continuously differentiable function and unit vector $\mathbf{g}$ denotes the polarization; the unit vector $\mathbf{n}$ defines the direction of wave propagation, and c is the phase velocity of the wave.

Substituting (9) into (8), we obtain

$$\mathbf{Q}(\mathbf{n})\cdot\mathbf{g} = \rho c^2\mathbf{g}, \tag{10}$$

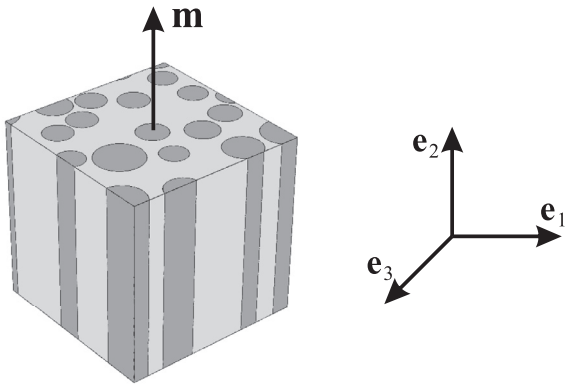


Fig. 1. Schematic representation of the FC with random distribution of fibers. ($\mathbf{e}_1$, $\mathbf{e}_2$, $\mathbf{e}_3$) is the orthonormal basis.

where

$$Q_{ij} = \mathcal{A}_{ijkl} n_j n_l \tag{11}$$

is the acoustic tensor defining the condition of propagation of the infinitesimal plane waves.

For incompressible materials Eq. (8) modifies as

$$\mathcal{A}_{ijkl} u_{k,lj} + \dot{p}_{,i} = \rho \frac{\partial^2 u_i}{\partial t^2}, \tag{12}$$

together with the incompressibility constraint

$$u_{i,i} = 0. \tag{13}$$

Substitution of (9) and $\dot{p} = p_0 h'(\mathbf{n}\cdot\mathbf{x} - ct)$, where p_0 is a scalar, into (12) and (13) yields

$$\hat{\mathbf{Q}}(\mathbf{n})\cdot\mathbf{g} = \rho c^2 \mathbf{g} \quad \text{and} \quad \mathbf{g}\cdot\mathbf{n} = 0, \tag{14}$$

where $\hat{\mathbf{Q}} = \hat{\mathbf{I}}\cdot\mathbf{Q}\cdot\hat{\mathbf{I}}$ and $\hat{\mathbf{I}} = \mathbf{I} - \mathbf{n}\otimes\mathbf{n}$ is the projection onto the plane normal to $\mathbf{n}$.

Next, let us consider a FC made out of aligned fibers embedded in a softer matrix with the volume fractions v_f and $v_m = 1 - v_f$. Here and thereafter, the fields and parameters of the constituents are denoted by the subscripts $(\bullet)_f$ and $(\bullet)_m$ for fibers and matrix, respectively. In the reference configuration the volume fractions of the phases can be calculated as

$$v_f = 1/\Omega \int_\Omega \eta_f(\mathbf{X}) d\mathbf{X} \quad \text{and} \quad v_m = 1/\Omega \int_\Omega \big(1 - \eta_f(\mathbf{X})\big) d\mathbf{X}, \tag{15}$$

where $\eta_f = 1$ if $\mathbf{X}$ is within the fiber phase and $\eta_f = 0$ otherwise; Ω is the volume occupied by the composite in the reference state. The macroscopic deformation gradient is defined as

$$\bar{\mathbf{F}} = 1/\Omega \int_\Omega \mathbf{F}(\mathbf{X}) d\mathbf{X}. \tag{16}$$

The *boundary conditions* for $\mathbf{F}_f$ and $\mathbf{F}_m$, and for $\mathbf{P}_f$ and $\mathbf{P}_m$ at the interfaces between the fibers and matrix are

$$\big(\mathbf{F}_f - \mathbf{F}_m\big)\cdot\mathbf{m} = \mathbf{0} \quad \text{and} \quad \big(\mathbf{P}_f - \mathbf{P}_m\big)\cdot\mathbf{w} = \mathbf{0}, \tag{17}$$

where the unit vector $\mathbf{m}$ denotes the initial fiber directions (see Fig. 1), and $\mathbf{w}$ is the arbitrary unit vector orthogonal to $\mathbf{m}$.

In this work, we consider fiber-reinforced materials with *incompressible* phases described by a neo-Hookean strain energy function (Ogden, 1997)

$$\psi_\xi^{inc} = \frac{\mu_\xi}{2}(\mathbf{F}_\xi : \mathbf{F}_\xi - 3), \tag{18}$$

where μ_ξ is the initial shear modulus. For a FC with incompressible neo-Hookean phases, an effective strain energy density function can be constructed (deBotton et al., 2006)

$$\psi(\bar{\mathbf{F}}) = \frac{\tilde{\mu}}{2}\big(\bar{\mathbf{F}} : \bar{\mathbf{F}} - 3\big) + \frac{\bar{\mu} - \tilde{\mu}}{2}\big(I_4 + 2I_4^{-1/2} - 3\big), \tag{19}$$

where $I_4 = \mathbf{m}\cdot\bar{\mathbf{C}}\cdot\mathbf{m}$, and $\bar{\mathbf{C}} = \bar{\mathbf{F}}^T\cdot\bar{\mathbf{F}}$ is the average right Cauchy-Green deformation tensor;

$$\bar{\mu} = v_f\mu_f + v_m\mu_m \quad \text{and} \quad \tilde{\mu} = \mu_m \frac{\big(1+v_f\big)\mu_f + v_m\mu_m}{v_m\mu_f + \big(1+v_f\big)\mu_m} \tag{20}$$

are the homogenized elastic moduli.

The acoustic tensor (14) corresponding to the strain energy function (19) takes the form

$$\hat{\mathbf{Q}}(\mathbf{n}, \bar{\mathbf{F}}) = q_1\hat{\mathbf{I}} + q_2\big(\hat{\mathbf{I}}\cdot\bar{\mathbf{F}}\cdot\mathbf{m}\big)\otimes\big(\hat{\mathbf{I}}\cdot\bar{\mathbf{F}}\cdot\mathbf{m}\big), \tag{21}$$

where

$$q_1 = \tilde{\mu}\big(\mathbf{n}\cdot\bar{\mathbf{B}}\cdot\mathbf{n}\big) + (\bar{\mu} - \tilde{\mu})\big(1 - I_4^{-3/2}\big)\big(\mathbf{n}\cdot\bar{\mathbf{F}}\cdot\mathbf{m}\big)^2 \tag{22}$$

and

$$q_2 = 3I_4^{-5/2}(\bar{\mu} - \tilde{\mu})\big(\mathbf{n}\cdot\bar{\mathbf{F}}\cdot\mathbf{m}\big)^2, \tag{23}$$

where $\bar{\mathbf{B}} = \bar{\mathbf{F}}\cdot\bar{\mathbf{F}}^T$ is the average left Cauchy–Green deformation tensor. The acoustic tensor (21) has the following nontrivial eigenvalues with the eigenvectors lying in the plane normal to $\mathbf{n}$

$$a_1 = q_1 \quad \text{and} \quad a_2 = q_1 + q_2\Big(I_4 - \big(\mathbf{n}\cdot\bar{\mathbf{F}}\cdot\mathbf{m}\big)^2\Big). \tag{24}$$

Thus, we have two distinct shear waves propagating in a finitely deformed incompressible FC with the corresponding phase velocities

$$\bar{c}_{sw}^{(1)} = \sqrt{\frac{a_1}{\bar{\rho}_0}} \quad \text{and} \quad \bar{c}_{sw}^{(2)} = \sqrt{\frac{a_2}{\bar{\rho}_0}}, \tag{25}$$

where $\bar{\rho}_0 = v_f\rho_{0f} + v_m\rho_{0m}$ is the average initial density of the FC.

The phase velocities of the shear waves (25) coincide only for special cases of applied deformations and directions of wave propagation. For instance, let us consider a uniaxially deformed FC with the corresponding macroscopic deformation gradient

$$\bar{\mathbf{F}} = \lambda\mathbf{e}_2\otimes\mathbf{e}_2 + \lambda^{-1/2}(\mathbf{I} - \mathbf{e}_2\otimes\mathbf{e}_2), \tag{26}$$

where λ is the applied macroscopic stretch ratio. Then, for waves propagating perpendicular to the fibers, i.e. $\mathbf{m} = \mathbf{e}_2$ and $\mathbf{n} = \mathbf{e}_1$, the phase velocities of the shear waves coincide

$$\bar{c}_{sw} = \bar{c}_{sw}^{(1)} = \bar{c}_{sw}^{(2)} = \sqrt{\frac{\tilde{\mu}}{\lambda\bar{\rho}_0}}. \tag{27}$$

The phase velocities also coincide for the waves propagating along the fibers, i.e. $\mathbf{n} = \mathbf{m} = \mathbf{e}_2$,

$$\bar{c}_{sw} = \bar{c}_{sw}^{(1)} = \bar{c}_{sw}^{(2)} = \lambda\sqrt{\frac{\bar{\mu} + (\tilde{\mu} - \bar{\mu})\lambda^{-3}}{\bar{\rho}_0}}. \tag{28}$$

However, for an oblique propagation of the waves relative to the fiber direction, for example, $\mathbf{m} = \mathbf{e}_2$ and $\mathbf{n} = (\mathbf{e}_1 + \mathbf{e}_2)/\sqrt{2}$, the phase velocities of the shear waves are distinct

$$\bar{c}_{sw}^{(1)} = \sqrt{\frac{2\tilde{\mu} + \big(\lambda^3 - 1\big)\bar{\mu}}{2\lambda\bar{\rho}_0}} \quad (\mathbf{g} = \mathbf{e}_3) \tag{29}$$

and

$$\bar{c}_{sw}^{(2)} = \sqrt{\frac{\tilde{\mu} + \bar{\mu}\big(1 + 2\lambda^3\big)}{4\lambda\bar{\rho}_0}} \quad \big(\mathbf{g} = (\mathbf{e}_2 - \mathbf{e}_1)/\sqrt{2}\big). \tag{30}$$

Note that (28) yields an explicit expression for the critical stretch ratio corresponding to the onset of macroscopic instability under uniaxial contraction (Rudykh and deBotton, 2012), namely

$$\lambda_{cr} = \left(1 - \frac{\tilde{\mu}}{\bar{\mu}}\right)^{1/3}. \tag{31}$$

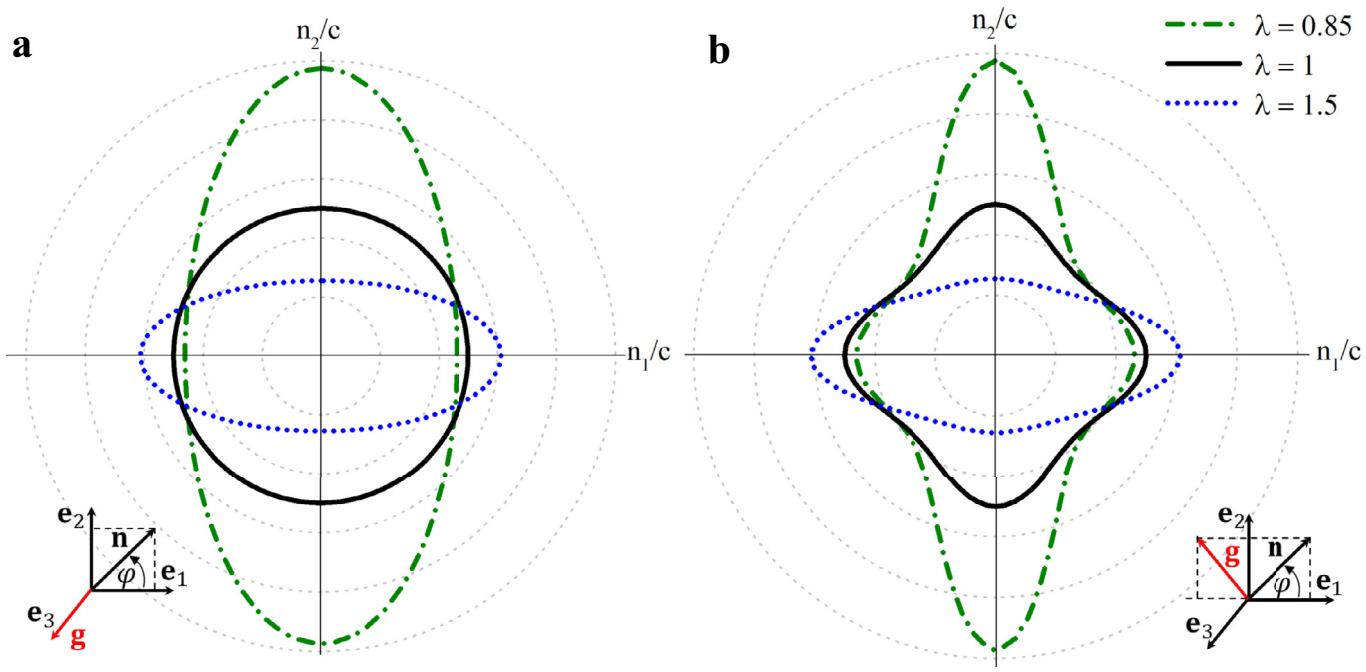


Fig. 2. Slowness curves for the out-of-plane (a) and in-plane (b) shear waves propagating in the FC with $\nu_f = 0.2$, $\mu_f/\mu_m = 10$, and $\rho_{0f}/\rho_{0m} = 1$ under uniaxial tension (26). Scale is 0.4 per division, and slowness is normalized by $\sqrt{\bar{\mu}/\bar{\rho}_0}$. Note that the horizontal and vertical axes with the corresponding labels n_1/c and n_2/c serve for showing the principal directions and physical quantity presented on the polar plot only.

To illustrate the influence of the deformation and direction of wave propagation on the characteristics of elastic waves in the FCs, we consider wave propagation in the plane $\langle \mathbf{e}_1, \mathbf{e}_2 \rangle$, i.e. $\mathbf{n} = \cos\varphi\ \mathbf{e}_1 + \sin\varphi\ \mathbf{e}_2$. By the use of the explicit relations (25) we construct the polar diagrams of slowness $\bar{s}_{sw}(\varphi) = 1/\bar{c}_{sw}(\varphi)$, also known in literature as slowness curves (Musgrave, 1970; Nayfeh, 1995). Fig. 2 shows an example of the slowness curves for the so-called out-of-plane (with polarization $\mathbf{g} = \mathbf{e}_3$) and in-plane (with polarization lying in plane $\langle \mathbf{e}_1, \mathbf{e}_2 \rangle$) shear waves in the FC undergoing uniaxial tension along the fibers. The examples are given for the FC with $\nu_f = 0.2$, $\mu_f/\mu_m = 10$, and the fiber direction $\mathbf{m} = \mathbf{e}_2$. The continuous black curves correspond to the undeformed FC, while the dash-dotted green and dotted blue curves are for the FC under the uniaxial contraction ($\lambda = 0.85$) and extension ($\lambda = 1.5$), respectively. Note that the critical stretch ratio for the considered FC undergoing uniaxial contraction is $\lambda_{cr} = 0.80$; therefore, the presented slowness curves for the compressed ($\lambda = 0.85$) FC correspond to a macroscopically stable state. The slowness curves clearly indicate the significant influence of the applied deformation on the shear wave propagation. Specifically, the contraction along the fibers results in a significant decrease of the phase velocities of the shear waves propagating in the direction of fibers; while the phase velocities increase for the waves propagating perpendicular to the fibers since these directions experience extension. Note that the phase velocity of the in-plane shear wave in the uniaxially deformed FC is maximal for certain directions of wave propagation $\mathbf{n}_0$. To find these directions, we substitute (26), $\mathbf{n}_0 = \cos\varphi_0\ \mathbf{e}_1 + \sin\varphi_0\ \mathbf{e}_2$, and $\mathbf{m} = \mathbf{e}_2$ into $(25)_2$, and then solve the extreme value problem for the phase velocity $\bar{c}^{(2)}_{sw}$ as a function of φ_0:

$$\varphi_0 = \pm\frac{1}{2}\arccos\left(\frac{1-\lambda^3}{3\left(1-\frac{\bar{\mu}}{\tilde{\mu}}\right)}\right) + \pi z,\ z = 0, 1. \tag{32}$$

In the undeformed state $\varphi_0 = \pm\frac{\pi}{4}, \pm\frac{3\pi}{4}$. Moreover, these directions differ from the principal directions in contrast to the out-of-plane shear wave – the phase velocity of which has the maxima in the directions of the principal axes. For example, in the uniaxially stretched FC the phase velocity of the out-of-plane shear wave is maximal for the wave propagation along the fibers, i.e. for $\mathbf{n} = \pm\mathbf{e}_2$ (see Fig. 2 (a)).

The dispersion relations for the long waves in an incompressible neo-Hookean FC are derived from (25) and have the following form

$$\bar{\omega}^{(1)}_{sw} = \sqrt{\frac{b_1}{\bar{\rho}_0}} \quad \text{and} \quad \bar{\omega}^{(2)}_{sw} = \sqrt{\frac{b_2}{\bar{\rho}_0}} \tag{33}$$

where

$$b_1 = \tilde{\mu}(\mathbf{k}\cdot\bar{\mathbf{B}}\cdot\mathbf{k}) + (\bar{\mu}-\tilde{\mu})\left(1-I_4^{-3/2}\right)\left(\mathbf{k}\cdot\bar{\mathbf{F}}\cdot\mathbf{m}\right)^2 \tag{34}$$

and

$$b_2 = b_1 + 3I_4^{-5/2}(\bar{\mu}-\tilde{\mu})\left(\mathbf{k}\cdot\bar{\mathbf{F}}\cdot\mathbf{m}\right)^2\left(I_4 - k^{-2}\left(\mathbf{k}\cdot\bar{\mathbf{F}}\cdot\mathbf{m}\right)^2\right), \tag{35}$$

where $\mathbf{k}$ is the wave vector and $k = |\mathbf{k}|$ is the wave number.

Hence, we can find the corresponding group velocity defined as

$$\mathbf{v}_g = \nabla_{\mathbf{k}}\omega. \tag{36}$$

Substitution of (33) into (36) yields explicit expressions for the group velocities of the long waves propagating in the finitely deformed FC

$$\mathbf{v}^{(1)}_{sw} = \frac{\left(\tilde{\mu}\bar{\mathbf{B}}\cdot\mathbf{n} + (\bar{\mu}-\tilde{\mu})\left(1-I_4^{-3/2}\right)\left(\mathbf{n}\cdot\bar{\mathbf{F}}\cdot\mathbf{m}\right)\bar{\mathbf{F}}\cdot\mathbf{m}\right)}{\sqrt{\bar{\rho}_0 a_1}} \tag{37}$$

and

$$\begin{aligned}\mathbf{v}^{(2)}_{sw} = \frac{1}{\sqrt{\bar{\rho}_0 a_2}}\Big(&\tilde{\mu}\bar{\mathbf{B}}\cdot\mathbf{n} + \\ &(\bar{\mu}-\tilde{\mu})\left(\mathbf{n}\cdot\bar{\mathbf{F}}\cdot\mathbf{m}\right)\Big[3I_4^{-5/2}\left(\mathbf{n}\cdot\bar{\mathbf{F}}\cdot\mathbf{m}\right)^3\mathbf{n} + \\ &\left(1+2I_4^{-3/2}\left(1-3I_4^{-1}\left(\mathbf{n}\cdot\bar{\mathbf{F}}\cdot\mathbf{m}\right)^2\right)\right)\bar{\mathbf{F}}\cdot\mathbf{m}\Big]\Big).\end{aligned} \tag{38}$$

In particular, the group velocities of the shear waves coincide for waves propagating perpendicular to the fibers (i.e. $\mathbf{m} = \mathbf{e}_2$ and $\mathbf{n} = \mathbf{e}_1$) in the uniaxially deformed FC

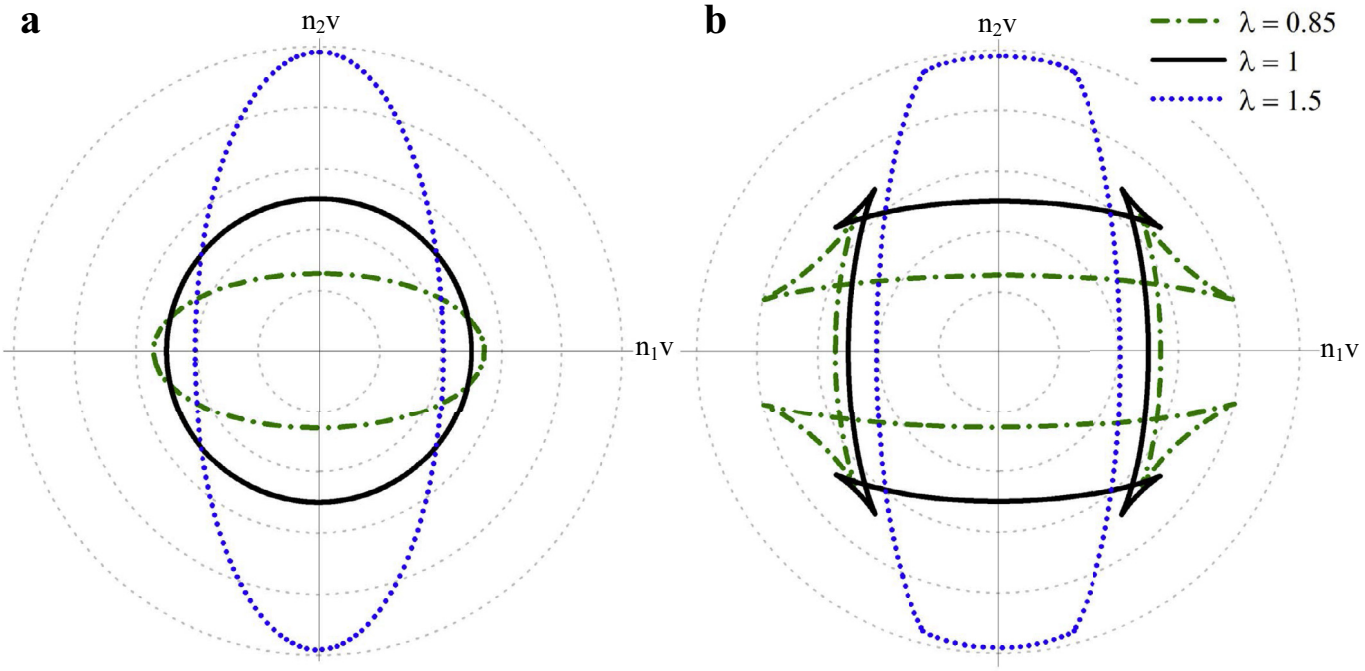


Fig. 3. Energy curves for (a) – out-of-plane and (b) – in-plane shear waves propagating in the FC with $\nu_f = 0.2$, $\mu_f/\mu_m = 10$, and $\rho_{0f}/\rho_{0m} = 1$ under uniaxial tension. Scale is 0.4 per division, where group velocity is normalized by $\sqrt{\bar{\rho}_0/\tilde{\mu}}$. Note that the horizontal and vertical axes with the corresponding labels (n_1v) and (n_2v) serve for showing the principal directions and physical quantity presented on the polar plot only.

$$\mathbf{v}_{sw}^{(1)} = \mathbf{v}_{sw}^{(2)} = \sqrt{\frac{\tilde{\mu}}{\lambda\bar{\rho}_0}}\,\mathbf{e}_1. \tag{39}$$

The group velocities also coincide for the waves propagating along the fibers, i.e. $\mathbf{n} = \mathbf{m} = \mathbf{e}_2$,

$$\mathbf{v}_{sw}^{(1)} = \mathbf{v}_{sw}^{(2)} = \lambda\sqrt{\frac{\bar{\mu} + (\tilde{\mu} - \bar{\mu})\lambda^{-3}}{\bar{\rho}_0}}\,\mathbf{e}_2. \tag{40}$$

To illustrate the derived results (37) and (38), we consider wave propagation in the plane $\langle \mathbf{e}_1, \mathbf{e}_2 \rangle$, i.e. $\mathbf{n} = \cos\varphi\ \mathbf{e}_1 + \sin\varphi\ \mathbf{e}_2$. Recall that the outer normal to the slowness curve shows the direction of the energy flow (Musgrave, 1970; Nayfeh, 1995). Hence, by assigning the absolute value of the group velocity (i.e. $|\mathbf{v}_{sw}|$) to the normal to the slowness curve for all possible propagation directions, the polar diagrams of group velocity or the energy curves (Musgrave, 1970; Nayfeh, 1995) are constructed. Fig. 3 shows an example of the energy curves for (a) out-of-plane and (b) in-plane shear waves propagating in the uniaxially deformed FC with $\nu_f = 0.2$, $\mu_f/\mu_m = 10$, and $\rho_{0f}/\rho_{0m} = 1$. The continuous black curves correspond to the undeformed FC while the dash-dotted green and dotted blue curves refer to the uniaxial contraction ($\lambda = 0.85$) and extension ($\lambda = 1.5$), respectively. Clearly, the group velocities of the shear waves strongly depend on the applied deformation and direction of wave propagation. Moreover, the energy curve of the in-plane shear wave has intersections, and their position can be manipulated by deformation (see Fig. 3 (b)). These intersections of the energy curves mean that the absolute values and directions of group velocity coincide for two different directions of wave propagation. For the out-of-plane shear wave the intersections are not observed (see Fig. 3 (a)). It is worth mentioning also that the energy curves of plane waves coincide with the wave fronts of impulsive point source excited waves in homogeneous anisotropic materials (Langenberg et al., 2010; Nayfeh, 1995). In this case, these cusps of energy curves will correspond to the regions of null energy (Nayfeh, 1995).

Next, let us consider slowness and energy curves near to, and at the onset of instability point. Fig. 4 shows the slowness curves of the shear waves propagating in the FC subjected to the uniaxial contraction of $\lambda = 0.81$ (dash-dotted green) and $\lambda = 0.80$ (dotted red), while $\lambda_{cr} = 0.80$. A comparison of Figs. 2 and 4 shows that the slowness of both shear waves propagating along the fibers dramatically increases (or phase velocity decreases) when the critical stretch is approached. In particular, in the FC contracted to $\lambda = 0.81$, the slownesses of shear waves propagating in the direction of fibers are 3.8 times larger than in the undeformed FC. Eventually, the slownesses tend to infinity in the FC contracted to the critical stretch ratio, i.e. at $\lambda = 0.80$. This is due to the fact that the phase velocities of the shear waves propagating along the fibers attain zero value in the FC subjected to $\lambda = \lambda_{cr}$ (see (28)). Lastly, Fig. 5 shows the energy curves of the shear waves propagating in the FC subjected to the uniaxial contraction of $\lambda = 0.81$ ((a) and (b)) and $\lambda = 0.80$ ((c) and (d)). We observe that the energy curve of the out-of-plane shear wave for the FC subjected to λ_{cr} degenerates into the three dots (see Fig. 5 (c)). The dot in the center means that the absolute value of the group velocity is zero for the wave propagating in direction of fibers (see (40)); the other two dots mean that the absolute value and direction of the group velocity do not change with the wave propagation direction. For the in-plane shear wave, the energy curve degenerates into the dot and two curved triangles (see Fig. 5 (d)). The dot in the center corresponds to the zero group velocity of the wave propagating along the fibers, while the curved triangles refer to the curvature of the corresponding slowness curve (see Fig. 4 (b)) in the vicinity of the wave propagation directions perpendicular to the fibers (i.e. $\mathbf{n} = \pm\mathbf{e}_1$).

4. Bloch wave analysis for wave propagation in 3D periodic FCs

To obtain the dispersion relations for finitely deformed 3D periodic FCs, we employ the Bloch wave analysis superimposed on a finite deformation (Aberg and Gudmundson, 1997; Bertoldi and Boyce, 2008b; 2008a; Rudykh and Boyce, 2014b). We implement

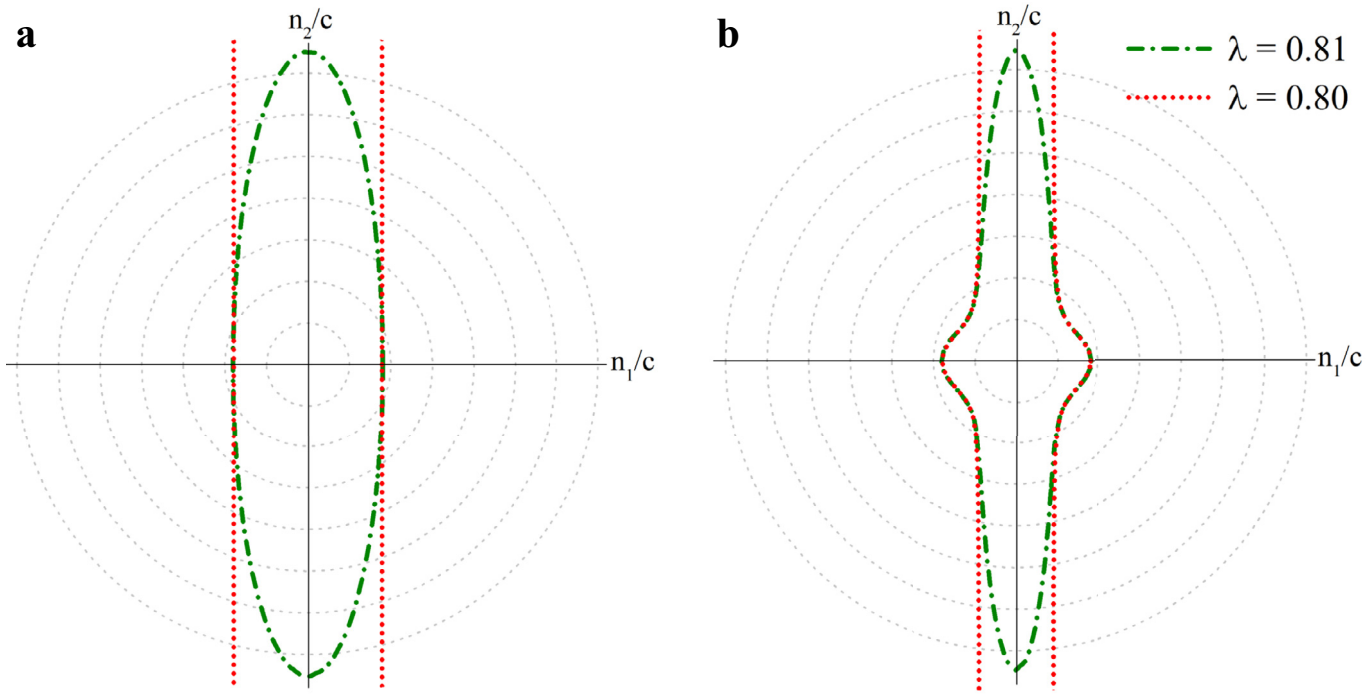


Fig. 4. Slowness curves for the out-of-plane (a) and in-plane (b) shear waves propagating in the FC with $\nu_f = 0.2$, $\mu_f/\mu_m = 10$, and $\rho_{0f}/\rho_{0m} = 1$ under uniaxial tension (26) near the instability. Scale is 0.5 per division, and slowness is normalized by $\sqrt{\tilde{\mu}/\tilde{\rho}_0}$.

the analysis in the finite element code. Fig. 6 shows an example of the corresponding representative volume element (RVE) for a FC with a square periodic unit cell. Geometrically, the fibers are characterized by their diameters, namely $d = 2a\sqrt{\nu_f/\pi}$, where a is the period of the FC (see Fig. 6). The periodic unit cell occupies a domain Ω in the undeformed configuration, namely

$$-a/2 \le x_1 \le a/2, \quad -h/2 \le x_2 \le h/2, \quad \text{and} \quad -a/2 \le x_3 \le a/2. \tag{41}$$

First, a solution for a finitely deformed state is obtained. The macroscopic deformation gradient $\bar{\mathbf{F}} = 1/\Omega \int_\Omega \mathbf{F} dV$ is applied through periodic boundary conditions imposed on the displacements of the RVE faces such that

$$\mathbf{U}_B - \mathbf{U}_A = \left(\bar{\mathbf{F}} - \mathbf{I}\right) \cdot (\mathbf{X}_B - \mathbf{X}_A) = \bar{\mathbf{H}} \cdot (\mathbf{X}_B - \mathbf{X}_A), \tag{42}$$

where A and B are the nodes on the opposite faces of the RVE boundary, $\bar{\mathbf{H}}$ is the average displacement gradient tensor, and $\mathbf{U} = \mathbf{x}(\mathbf{X}) - \mathbf{X}$ is the displacement field. The macroscopic first Piola–Kirchhoff stress tensor and the corresponding Cauchy stress tensor are calculated as $\bar{\mathbf{P}} = 1/\Omega \int_\Omega \mathbf{P} dV$ and $\bar{\boldsymbol{\sigma}} = 1/\Omega \int_\Omega \boldsymbol{\sigma} dV$, respectively. Rigid body motions are prevented by fixing the displacements of a single node. Although the analysis is general and it can be applied for materials subjected to any macroscopically applied homogeneous deformation $\bar{\mathbf{F}}$, here the examples are given for a uniaxial loading (26).

Second, the Bloch wave analysis is performed for the finitely deformed state. The corresponding incremental change in the displacement and the first Piola–Kirchhoff stress tensor can be expressed as

$$\mathbf{u}(\mathbf{X}, t) = \dot{\boldsymbol{\kappa}}(\mathbf{X}) e^{-i\omega t} \quad \text{and} \quad \dot{\mathbf{P}} = \dot{\mathcal{P}} e^{-i\omega t}, \tag{43}$$

where ω is the angular frequency. By substitution (43) in (5), we obtain

$$\mathrm{Div}\dot{\mathcal{P}} + \rho_0 \omega^2 \dot{\boldsymbol{\kappa}} = \mathbf{0}. \tag{44}$$

According to the Floquet theorem (Kittel, 2004)

$$\dot{\boldsymbol{\kappa}}(\mathbf{X} + \mathbf{R}) = \dot{\boldsymbol{\kappa}}(\mathbf{X}) e^{-i\mathbf{K}^0 \cdot \mathbf{R}}, \tag{45}$$

where $\mathbf{R}$ defines the distance between the nodes on the opposite faces of the RVE in the reference configuration. The periodicity conditions (45) are imposed in the finite element code through the corresponding boundary conditions for the displacements of the opposite faces (Slesarenko and Rudykh, 2017; Bertoldi and Boyce, 2008a; 2008b; Wang and Bertoldi, 2012). The dispersion relations are obtained by solving the eigenvalue problem stemming from Eqs. (43)–(45) for a range of the wave vectors $\mathbf{K}^0$.

We start from comparing the results of the Bloch wave numerical analysis and the analytical estimates (33) for the long wave limit. Fig. 7 presents the comparisons for the wave propagating in the direction of fibers. The FCs are subjected to the uniaxial tension (26) along the fiber direction of the magnitude $\lambda = 1.25$. Fig. 7 (a) and (b) show the comparison for FCs with $\nu_f = 0.25$, $\mu_f/\mu_m = 10$ and $\mu_f/\mu_m = 1000$, respectively; while Fig. 7 (c) and (d) show the comparison for FCs with $\nu_f = 0.01$, $\mu_f/\mu_m = 10$ and $\mu_f/\mu_m = 1000$, respectively. The continuous black curves refer to the numerical simulations while the dashed red curves correspond to the long wave estimates (33). Here and thereafter, we consider FCs with constituents having identical densities (i.e. $\rho_{0f}/\rho_{0m} = 1$), and frequency is normalized as $f_n = fa\sqrt{\tilde{\rho}_0/\tilde{\mu}}$, where $f = \omega/(2\pi)$. Fig. 7 (a) and (c) show that the long wave estimates are in excellent agreement with the results of numerical simulations up to the wavelengths comparable with the period a of the unit cell for FCs possessing a small amount of fibers and a moderate contrast in the shear modulus between the constituents. However, for larger contrasts in the shear moduli, the long wave estimates are in good agreement with the Bloch wave analysis only for wavelengths significantly exceeding the period of the unit cell, namely $l \gtrsim \pi^2 a$ (see Fig. 7 (b) and (d)). Thus, the difference between the long wave estimates (33) and Bloch wave analysis increases with an increase in the volume fraction and shear modulus of fibers (i.e. the role of the fibers becomes more significant).

Fig. 8 presents the dispersion curves for the periodic FCs with $\nu_f = 0.25$ and (a) $\mu_f/\mu_m = 10$, (b) $\mu_f/\mu_m = 100$, and (c) $\mu_f/\mu_m = 1000$ undergoing uniaxial deformations along the fibers.

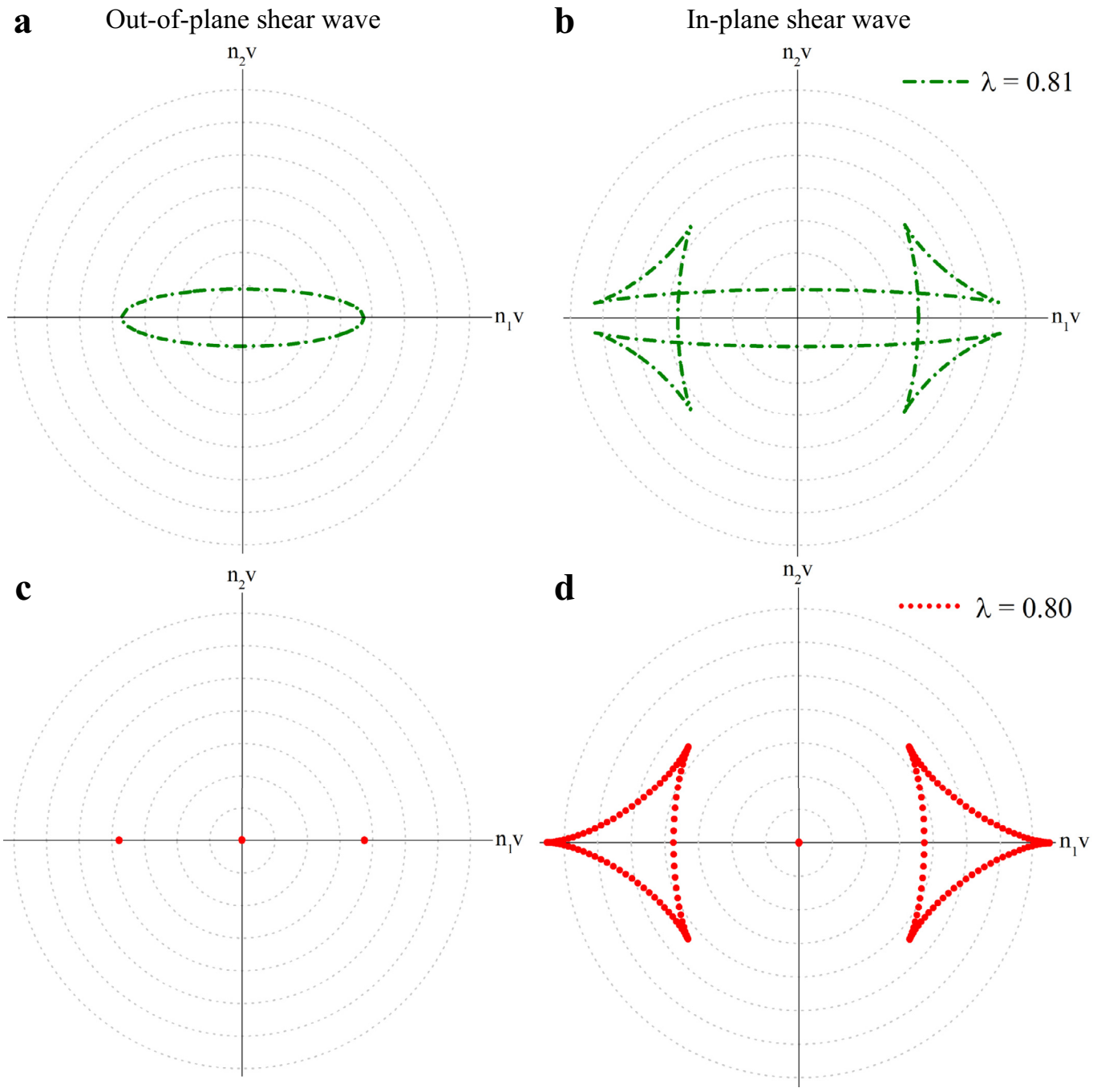


Fig. 5. Energy curves for the out-of-plane (a, c) and in-plane (b, d) shear waves propagating in the FC with $\nu_f = 0.2$, $\mu_f/\mu_m = 10$, and $\rho_{0f}/\rho_{0m} = 1$ under uniaxial tension (26) near the instability. Scale is 0.3 per division, and group velocity is normalized by $\sqrt{\tilde{\rho}_0/\tilde{\mu}}$.

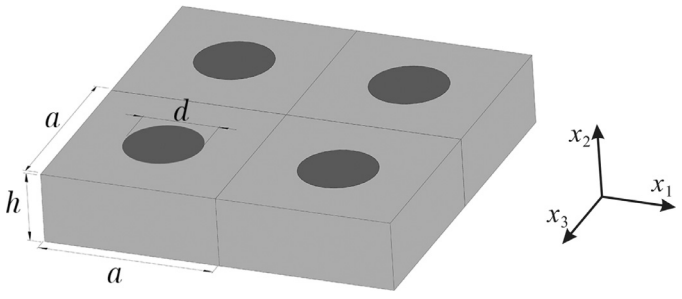


Fig. 6. RVE for a 3D periodic FC with a square arrangement of fibers.

The dispersion curves presented in Fig. 8 (and also in Fig. 9) are obtained by utilizing the Bloch wave analysis implemented in the finite element code. Clearly, for the FC with the low shear modulus contrast between the fibers and matrix (e.g., $\mu_f/\mu_m = 10$), the deformation slightly influences dispersion curves (Fig. 8 (a)). However, the influence of deformation increases for the FCs with moderate and high shear modulus contrasts (e.g., $\mu_f/\mu_m = 100$ and $\mu_f/\mu_m = 1000$). Specifically, deformation considerably influences the dispersion of the waves with wavelengths exceeding the characteristic length-scale of the FC (Fig. 8 (b) and (c)). For example, for the wavenumber $ka/(2\pi) = 0.2$, the uniaxial tension of the magnitude $\lambda = 1.5$ shifts the dispersion curve from $f_n = 0.29$ up to

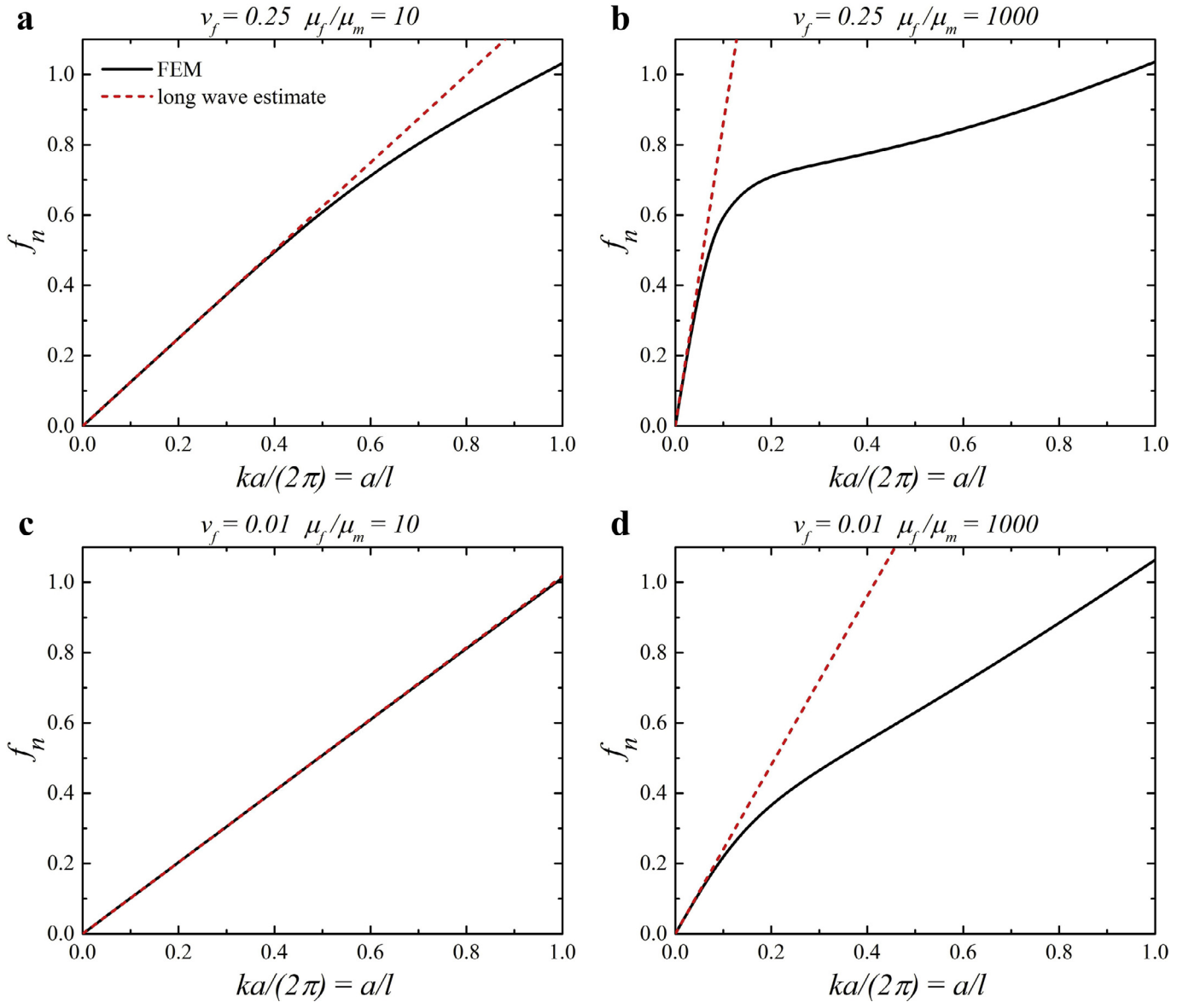


Fig. 7. Comparison of the long wave estimates (33) and the Bloch wave numerical analysis for the shear waves propagating in the direction of fibers. Periodic FCs with $v_f = 0.25$ and (a) $\mu_f/\mu_m = 10$, (b) $\mu_f/\mu_m = 1000$, and $v_f = 0.01$ and (c) $\mu_f/\mu_m = 10$, (d) $\mu_f/\mu_m = 1000$ are subjected to the uniaxial tension along the fiber direction, $\lambda = 1.25$. Frequency is normalized as $f_n = \frac{\omega a}{2\pi}\sqrt{\tilde{\rho}_0/\tilde{\mu}}$.

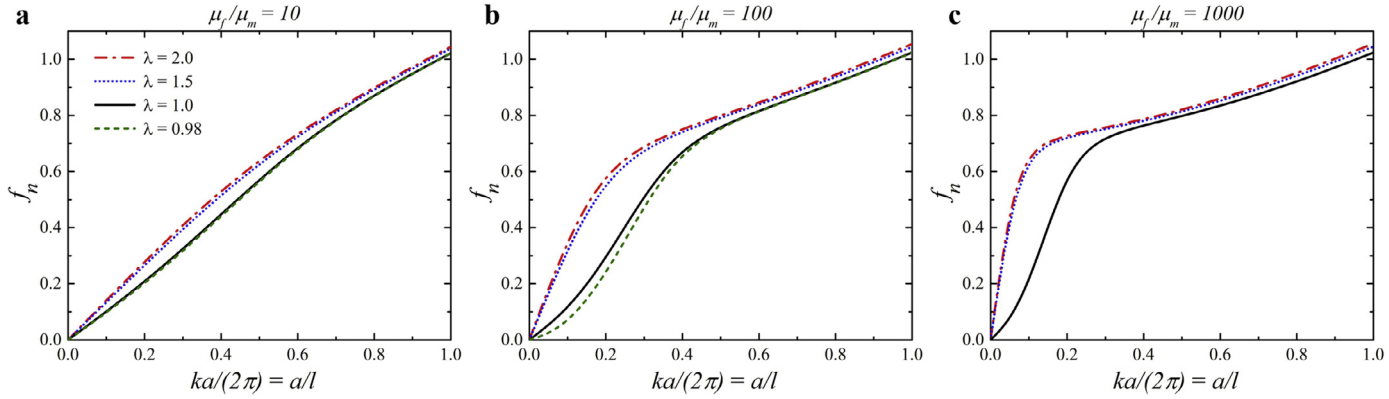


Fig. 8. Dispersion curves for the shear waves propagating in the direction of fibers in FCs with $v_f = 0.25$ and (a) $\mu_f/\mu_m = 10$, (b) $\mu_f/\mu_m = 100$, and (c) $\mu_f/\mu_m = 1000$. The FCs are subjected to the uniaxial tension of the magnitude $\lambda = 0.98$ (dashed green curves), $\lambda = 1$ (continuous black curves), $\lambda = 1.5$ (dotted blue curves), and $\lambda = 2$ (dash-dotted red curves). Frequency is normalized as $f_n = \frac{\omega a}{2\pi}\sqrt{\tilde{\rho}_0/\tilde{\mu}}$. (For interpretation of the references to colour in this figure legend, the reader is referred to the web version of this article.)

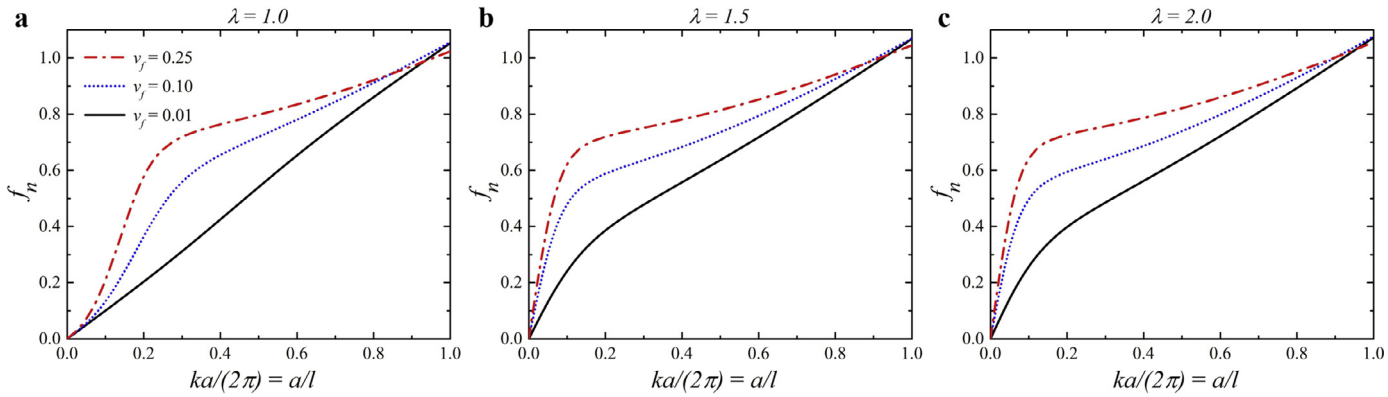


Fig. 9. Dispersion curves for shear waves propagating in the direction of fibers in FCs with $\mu_f/\mu_m = 1000$ in the undeformed state (a) and for the FCs subjected to the uniaxial tension of magnitude $\lambda = 1.5$ (b) and $\lambda = 2$ (c).

$f_n = 0.55$ as compared to the response of the undeformed FC with $v_f = 0.25$ and $\mu_f/\mu_m = 100$ (Fig. 8 (b)). Remarkably, the dispersion curves for the short waves (i.e. $l \lesssim 2a$) are barely affected by the uniaxial deformation (Fig. 8 (b) and (c)). Moreover, the dispersion curves change more slowly with deformation after a certain level of stretch is reached (compare dash-dotted red and dotted blue curves in Fig. 8). This happens because the phase velocities (28) of the long shear waves start to change slowly when a certain level of deformation is achieved.

To clarify the influence of the deformation on the dispersion phenomenon in FCs with various volume fractions of the fibers, we present dispersion curves for FCs with $\mu_f/\mu_m = 1000$ in the undeformed state (a) and for the FCs subjected to the uniaxial tension of magnitude $\lambda = 1.5$ (b) and $\lambda = 2$ (c) in Fig. 9. The continuous black, dotted blue, and dashed-dotted red curves correspond to $v_f = 0.01$, $v_f = 0.10$, and $v_f = 0.25$, respectively. We observe that the dispersion of shear waves in the fiber direction is more pronounced for the periodic FCs with large volume fractions of fibers (compare continuous black and dash-dotted red curves in Fig. 9 (a)). Moreover, a uniaxial extension of the periodic FCs along the fibers significantly affects dispersion curves (Fig. 9 (b) and (c)); however, an increase in the loading leads to a moderate change in the dispersion curve after a certain level of deformation (compare Fig. 9 (b) and (c)). For example, the frequency of the shear wave with $ka/(2\pi) = 0.1$ propagating in the FC with $v_f = 0.25$ and $\mu_f/\mu_m = 1000$ increases from $f_n = 0.21$ in the undeformed FC up to $f_n = 0.64$ in the FC subjected to the uniaxial tension of the magnitude $\lambda = 1.5$ while it increases only up to $f_n = 0.66$ in the FC subjected to the uniaxial tension of the magnitude $\lambda = 2$ (compare dash-dotted red curves in Fig. 9). This is due to the fact that the phase velocities (28) of long shear waves change more slowly after a certain level of deformation is reached.

Finally, we consider the influence of the fiber arrangement on the shear wave propagation in the direction of fibers. Fig. 10 shows an example of RVE for a FC with a rectangular periodic unit cell. Geometrically, the fibers are characterized by their diameters, namely $d = 2\sqrt{abv_f/\pi}$ (see Fig. 10). The periodic unit cell occupies a domain Ω in the undeformed configuration, namely

$$-a/2 \le x_1 \le a/2, \quad -h/2 \le x_2 \le h/2, \quad \text{and} \quad -b/2 \le x_3 \le b/2. \tag{46}$$

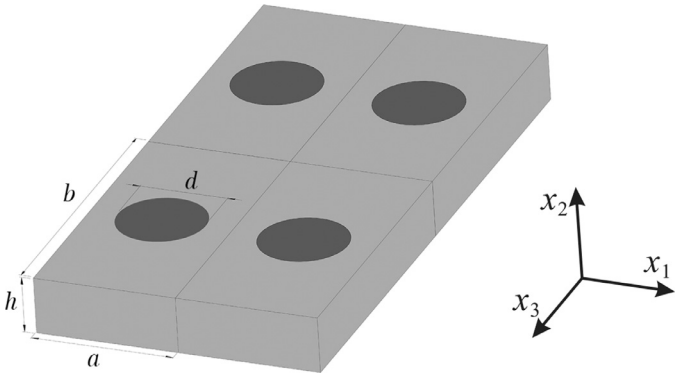


Fig. 10. RVE for a 3D periodic FC with a rectangular arrangement of fibers.

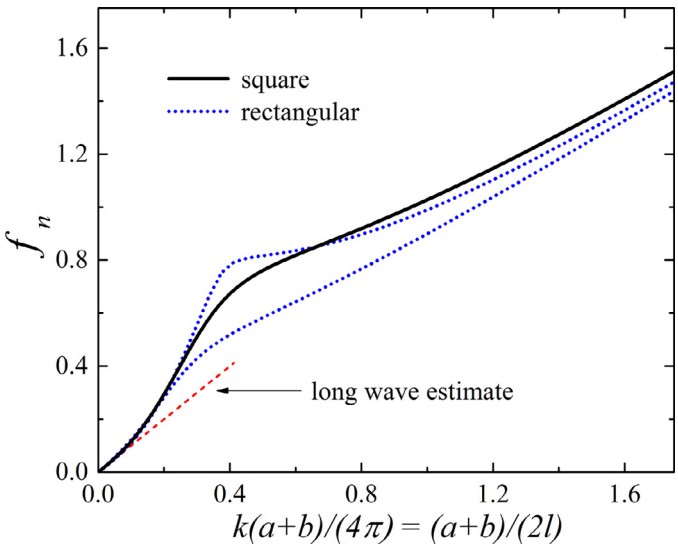


Fig. 11. Dispersion curves for shear waves propagating in the direction of fibers in FCs with $v_f = 0.25$ and $\mu_f/\mu_m = 100$ in the undeformed state with square and rectangular ($b = 2a$) arrangements of fibers.

Fig. 11 presents a comparison of the dispersion curves for shear waves propagating along the fibers in the FC with the square and rectangular ($b = 2a$) arrangements of the fibers. The dispersion curves of the shear waves vary in the FC with rectangular arrangement of fibers, because we have two distinct characteristic lengths, namely a and b, as opposite to the square arrangement. We compare FCs with the same volume fractions of fibers (i.e. $v_f = 0.25$); as a result, the dispersion curves of the long shear waves (i.e. $l \gtrsim 5(a+b)/2$) coincide for both square and rectangular periodic FCs. Consistently with the previous observations, a significant nonlinearity of dispersion curves is observed for the shear waves with wavelengths being comparable to the characteristic lengths of the

FC, namely $l \sim (a+b)$. The dispersion curves for shorter waves (i.e. $l \lesssim (a+b)/3$) are affected only slightly by the fiber arrangement.

5. Concluding remarks

We considered the shear wave propagation in the 3D fiber-reinforced composites undergoing finite deformations. First, we derived the explicit closed form expressions for the phase and group velocities of the shear waves propagating in the finitely deformed 3D FCs on the basis of a micromechanical approach accounting for the material properties and distribution of the phases. Hence, the derived explicit relations for the phase and group velocities were expressed in terms of the actual mechanical properties of composite constituents and their volume fractions. By utilizing these expressions, we constructed the slowness and energy curves revealing the strong influence of deformation on the propagation of shear waves. In particular, the shear wave velocities were shown to vary considerably with the deformation and direction of wave propagation. Moreover, the energy curve of the in-plane shear wave was shown to have deformation tunable intersections, meaning that the absolute values and directions of the group velocities coincide for the different directions of wave propagation. Thus, we are able to estimate characteristics of wave and energy propagation in the finitely deformed 3D fiber composites employing these explicit relations, which are applicable for any direction of wave propagation and for any macroscopically applied homogeneous pre-deformation. These important characteristics are expressed in terms of the actual microstructure parameters, such as volume fractions and phase material properties. This important feature distinguishes our results from those derived from phenomenological models, where the material parameters need to be fitted, and they are not directly related to the microstructure parameters and material properties of the constituents.

Second, we examined the shear wave propagation in the finitely deformed 3D periodic FCs by application of the Bloch wave approach in the finite element code. This allowed us to account for the interactions of the elastic waves with the material microstructure. As a result, we found the dispersion phenomenon manifesting in the strongly nonlinear dependence of the wave frequencies on wavenumber. The dispersion and the corresponding wavelengths of the shear waves in the 3D periodic FCs were found to be tunable by the change in the shear modulus contrast between the constituents and volume fraction of the fibers. Specifically, an increase in the shear modulus contrast and amount of fibers leads to a more pronounced dispersion of shear waves propagating in the direction of fibers, i.e. the dispersion curves exhibit a significant nonlinearity. Moreover, the dispersion of shear waves is highly sensitive to deformation. In particular, a moderate deformation significantly increases the frequency of the long waves. However, the influence of deformation for the short waves is relatively weak. We found that the influence of deformation on the dispersion of shear waves is more pronounced at the beginning of the loading due to the fact that the phase velocities (28) of the long shear waves change quickly up to a certain level of deformation and then the phase velocities vary slowly with a further loading. Next, we compared the results of the Bloch wave analysis and the long wave estimates. We found that the long wave estimates for the phase velocities (25) of shear waves accurately describe the dispersion relations for the finitely deformed FCs with low shear modulus contrast between the fibers and matrix (i.e. $\mu_f/\mu_m \lesssim 10$) and small volume fractions of the fibers (i.e. $v_f \lesssim 0.25$).

Finally, we analyzed the influence of the fiber arrangement on the propagation of shear waves along the fibers. In particular, by comparing dispersion curves of shear waves for FCs with square and rectangular arrangements of fibers, we observed that (i) long shear waves are independent of the fiber arrangement, (ii) shear waves with wavelengths being comparable to the characteristic lengths of the FC are significantly affected by the fiber arrangement, and (iii) short shear waves are affected only slightly by the fiber arrangement.

Acknowledgments

This work was supported by the Israel Science Foundation (grant №1550/15 and 1973/15). Stephan Rudykh gratefully acknowledges the support of Taub Foundation through the Horev Fellowship – Leaders in Science and Technology. Viacheslav Slesarenko thanks the support through the Technion Postdoctoral Fellowship.

References

Aberg, M., Gudmundson, P., 1997. The usage of standard finite element codes for computation of dispersion relations in materials with periodic microstructure. J. Acoust. Soc. Am. 102, 2007–2013.
Babaee, S., Shim, J., Weaver, J., Chen, E., Patel, N., Bertoldi, K., 2013. 3D soft metamaterials with negative poisson's ratio. Adv. Mater. 25 (36), 5044–5049.
Babaee, S., Viard, N., Wang, P., Fang, N.X., Bertoldi, K., 2016. Harnessing deformation to switch on and off the propagation of sound. Adv. Mater. 28 (8), 1631–1635.
Bafekrpour, E., Molotnikov, A., Weaver, J.C., Brechet, Y., Estrin, Y., 2014. Responsive materials: a novel design for enhanced machine-augmented composites. Sci. Rep. 4, 5801–5821.
Bertoldi, K., Boyce, M.C., 2008a. Mechanically triggered transformations of phononic band gaps in periodic elastomeric structures. Phys. Rev. B 77 (5), 052105.
Bertoldi, K., Boyce, M.C., 2008b. Wave propagation and instabilities in monolithic and periodically structured elastomeric materials undergoing large deformations. Phys. Rev. B 78, 184107.
Bertoldi, K., Boyce, M.C., Deschanel, S., Prange, S., Mullin, T., 2008. Mechanics of deformation-triggered pattern transformations and superelastic behavior in periodic elastomeric structures. J. Mech. Phys. Solids 56 (8), 2642–2668.
Biot, M.A., 1939. Non Linear Theory of Elasticity and the linearized case for a body under initial stress. Philos. Mag. XXVII, 468–489.
Biot, M.A., 1940. The influence of initial stress on elastic waves. J. Appl. Phys. 11 (8), 522.
Boulanger, P., Hayes, M., 1992. Finite-amplitude waves in deformed mooney-rivlin materials. Q. J. Mech. Appl. Math. 45 (4), 575–593.
Boulanger, P., Hayes, M., Trimarco, C., 1994. Finite-amplitude plane waves in deformed hadamard elastic materials. Geophys. J. Int. 118 (2), 447–458.
Celli, P., Gonella, S., 2015. Manipulating waves with LEGO® bricks: a versatile experimental platform for metamaterial architectures. Appl. Phys. Lett. 107, 081901.
Chen, Q., Elbanna, A., 2016. Modulating elastic band gap structure in layered soft composites using sacrificial interfaces. J. Appl. Mech. 83, 111009.
Currie, P., Hayes, M., 1969. Longitudinal and transverse waves in finite elastic strain. hadamard and green materials. IMA J. Appl. Math. 5 (2), 140–161.
deBotton, G., Hariton, I., Socolsky, E.A., 2006. Neo-Hookean fiber-reinforced composites in finite elasticity. J. Mech. Phys. Solids 54, 533–559.
Destrade, M., Ogden, R.W., 2013. On stress-dependent elastic moduli and wave speeds. J. Appl. Math. 78 (5), 965–997.
Dorfmann, A., Ogden, R.W., 2010. Electroelastic waves in a finitely deformed electroactive material. IMA J. Appl. Math. 75 (4), 603–636.
Fomenko, S.I., Golub, M.V., Zhang, C., Bui, T.Q., Wang, Y.-S., 2014. In-plane elastic wave propagation and band-gaps in layered functionally graded phononic crystals. Int. J. Solids Struct. 51, 2491–2503.
Galich, P.I., Fang, N.X., Boyce, M.C., Rudykh, S., 2017. Elastic wave propagation in finitely deformed layered materials. J. Mech. Phys. Solids 98, 390–410.
Galich, P.I., Rudykh, S., 2015a. Comment on "Disentangling longitudinal and shear elastic waves by neo-Hookean soft devices". Appl. Phys. Lett. 107, 056101. 106, 161903.
Galich, P.I., Rudykh, S., 2015b. Influence of stiffening on elastic wave propagation in extremely deformed soft matter: from nearly incompressible to auxetic materials. Extreme Mech. Lett. 4, 156–161.
Galich, P.I., Rudykh, S., 2016. Manipulating pressure and shear elastic waves in dielectric elastomers via external electric stimuli. Int. J. Solids Struct. 91, 18–25.
Ge, Q., Qi, H.J., Dunn, M.L., 2013. Active materials by four-dimension printing. Appl. Phys. Lett. 103 (13), 131901.
Gei, M., 2008. Elastic waves guided by a material interface. Eur. J. Mech. 27 (3), 328–345.
Golub, M.V., Fomenko, S.I., Bui, T.Q., Zhang, C., Wang, Y.-S., 2012. Transmission and band gaps of elastic SH waves in functionally graded periodic laminates. Int. J. Solids Struct. 49, 344–354.
Humphrey, J.D., 2002. Cardiovascular Solid Mechanics: Cells, Tissues, and Organs. Springer-Verlag, New York.
John, F., 1966. Plane elastic waves of finite amplitude. hadamard materials and harmonic materials. Commun. Pure Appl. Math. 19 (3), 309–341.
Kittel, C., 2004. Introduction to Solid State Physics. Wiley, Hoboken, N.J.
Kolle, M., Lethbridge, A., Kreysing, M., Baumberg, J., Aizenberg, J., Vukusic, P., 2013. Bio-inspired band-gap tunable elastic optical multilayer fibers. Adv. Mater. 25 (15), 2239–2245.

Kushwaha, M., Halevi, P., Dobrzynski, L., Djafari-Rouhani, B., 1993. Acoustic band structure of periodic elastic composites. Phys. Rev. Lett. 71 (13), 2022–2025.
Langenberg, K.J., Marklein, R., Mayer, K., 2010. Energy vs. group velocity for elastic waves in homogeneous anisotropic solid media. In: Proceedings of 2010 URSI International Symposium on Electromagnetic Theory, pp. 733–736.
Li, Y., Kaynia, N., Rudykh, S., Boyce, M.C., 2013. Wrinkling of interfacial layers in stratified composites. Adv. Eng. Mater. 15 (10), 921–926.
Lin, E., Li, Y., Ortiz, C., Boyce, M.C., 2014. 3D printed, bio-inspired prototypes and analytical models for structured suture interfaces with geometrically-tuned deformation and failure behavior. J. Mech. Phys. Solids 73, 166–182.
Musgrave, M.J.P., 1970. Crystal Acoustics: Introduction to the Study of Elastic Waves and Vibrations in Crystals. Holden-day, San Francisco.
Nayfeh, A.H., 1995. Wave Propagation in Layered Anisotropic Media: With Applications to Composites. Elsevier Science, Amsterdam.
Ogden, R., Singh, B., 2011. Propagation of waves in an incompressible transversely isotropic elastic solid with initial stress: biot revisited. J. Mech. Mater. Struct. 6 (1–4), 453–477.
Ogden, R.W., 1997. Non-linear Elastic Deformations. Dover Publications, New York.
Rogerson, G., Scott, N., 1994. Doubly constrained elastic wave propagation. Int. J. Solids Struct. 31 (20), 2769–2792.
Rudykh, S., Boyce, M., 2014a. Transforming small localized loading into large rotational motion in soft anisotropically-structured materials. Adv. Eng. Mater. 16 (11), 1311–1317.
Rudykh, S., Boyce, M., 2014b. Transforming wave propagation in layered media via instability-induced interfacial wrinkling. Phys. Rev. Lett. 112, 034301.
Rudykh, S., deBotton, G., 2012. Instabilities of hyperelastic fiber composites: micromechanical versus numerical analyses. J. Elasticity 106, 123–147.
Rudykh, S., Ortiz, C., Boyce, M., 2015. Flexibility and protection by design: imbricated hybrid microstructures of bio-inspired armor. Soft Matter 11, 2547–2554.
Saheb, D.N., Jog, J.P., 1999. Natural fiber polymer composites: a review. Adv. Polym. Technol. 18 (4), 351–363.
Scott, N., 1991. Small vibrations of prestrained constrained elastic materials: the idealized fibre-reinforced material. Int. J. Solids Struct. 27 (15), 1969–1980.
Scott, N., 1992. Waves in a homogeneously prestrained incompressible, almost inextensible, fibre-reinforced elastic material. Proc. R. Irish Acad. Sect. A 92A (1), 9–36.
Scott, N., Hayes, M., 1976. Small vibrations of a fibre-reinforced composite. Q. J. Mech. Appl. Math. 29 (4), 467–486.
Slesarenko, V., Rudykh, S., 2016. Harnessing viscoelasticity and instabilities for tuning wavy patterns in soft layered composites. Soft Matter 12, 3677–3682.
Slesarenko, V., Rudykh, S., 2017. Microscopic and macroscopic instabilities in hyperelastic fiber composites. J. Mech. Phys. Solids doi:10.1016/j.jmps.2016.11.002.
Srivastava, A., 2016. Metamaterial properties of periodic laminates. J. Mech. Phys. Solids 96, 252–263.
Truesdell, C., Noll, W., 1965. The Non-Linear Field Theories of Mechanics. Springer.
Wang, L., Bertoldi, K., 2012. Mechanically tunable phononic band gaps in three-dimensional periodic elastomeric structures. Int. J. Solids Struct. 49 (19–20), 2881–2885.

Update

International Journal of Solids and Structures
Volume 135, Issue , 15 March 2018, Page 303–304

DOI: https://doi.org/10.1016/j.ijsolstr.2017.12.027

International Journal of Solids and Structures 135 (2018) 303–304

Contents lists available at ScienceDirect

International Journal of Solids and Structures

journal homepage: www.elsevier.com/locate/ijsolstr

Corrigendum to "Shear wave propagation in finitely deformed 3D fiber-reinforced composites" [Int. J. Solids Struct. 110–111 (2017) 294–304]

Pavel I. Galich, Viacheslav Slesarenko, Stephan Rudykh*

Department of Aerospace Engineering, Technion – Israel Institute of Technology, Haifa 32000, Israel

In our paper (Galich et al., 2017), Figs. 7–9 show frequencies as functions of wavenumber K^0 (in the undeformed configuration); thus, in Figs. 7–9, $K^0 = |\mathbf{K}^0|$ must replace $k = |\mathbf{k}|$ (in the deformed configuration). Recall that the corresponding wave vectors in the undeformed

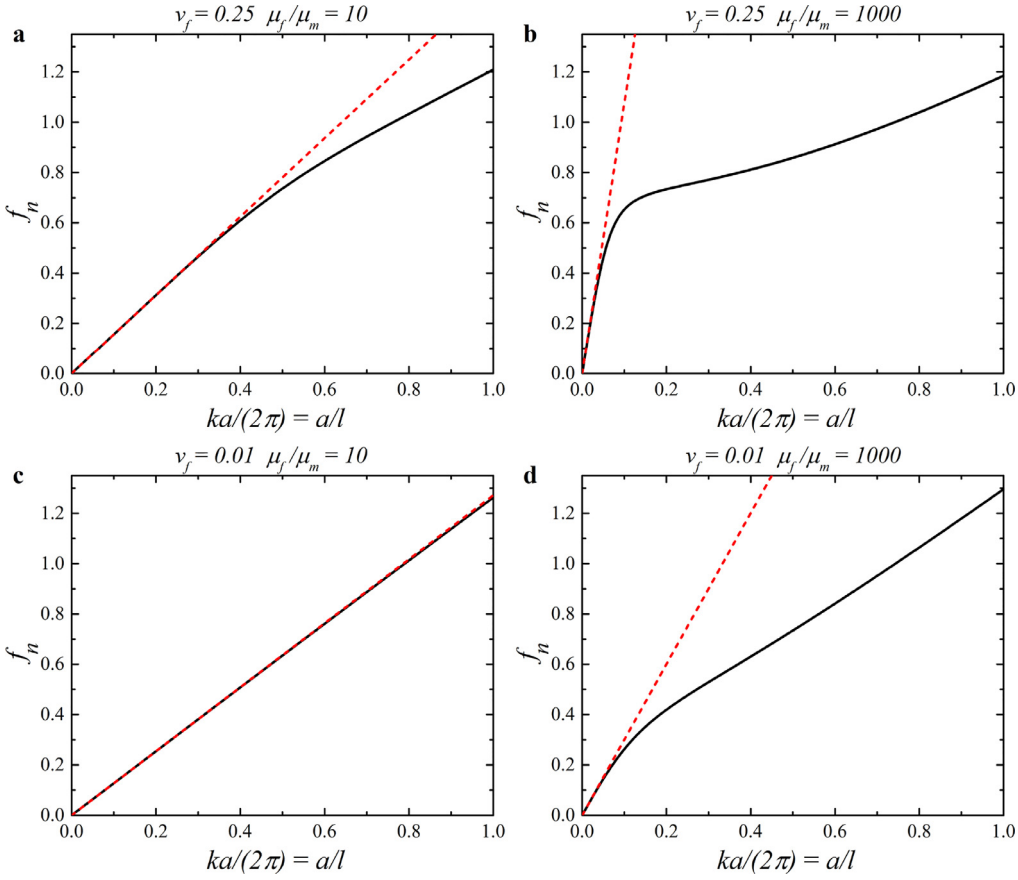


Fig. 1. Comparison of the long wave estimates (33) and the Bloch wave numerical analysis for the shear waves propagating in the direction of fibers. Periodic FCs with $v_f = 0.25$ and (a) $\mu_f/\mu_m = 10$, (b) $\mu_f/\mu_m = 1000$, and $v_f = 0.01$ and (c) $\mu_f/\mu_m = 10$, (d) $\mu_f/\mu_m = 1000$ are subjected to the uniaxial tension along the fiber direction, $\lambda = 1.25$. Frequency is normalized as $f_n = \frac{\omega a}{2\pi}\sqrt{\tilde{\rho}_0/\tilde{\mu}}$.

DOI of original article: 10.1016/j.ijsolstr.2016.12.007

* Corresponding author.
E-mail address: rudykh@technion.ac.il (S. Rudykh).

https://doi.org/10.1016/j.ijsolstr.2017.12.027
0020-7683

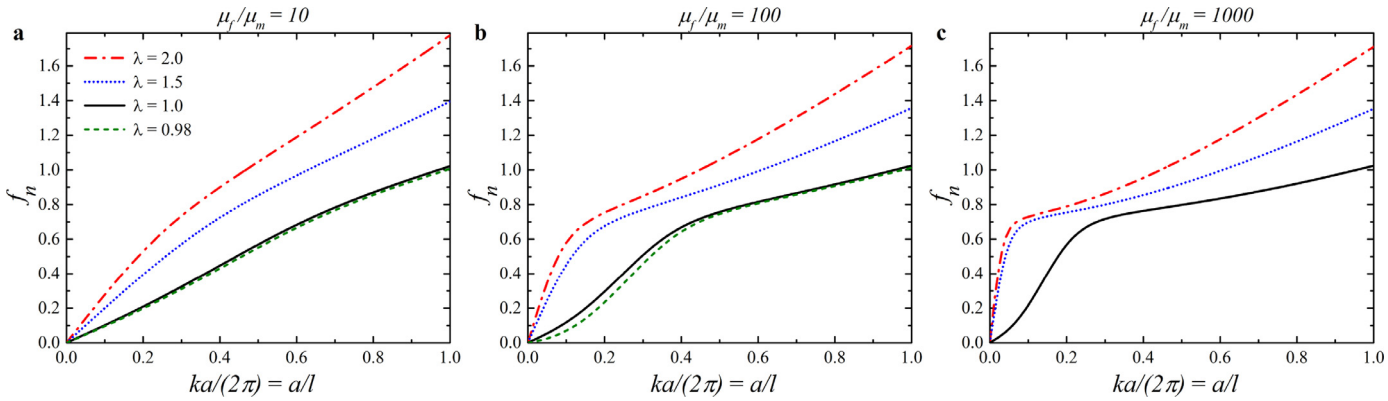


Fig. 2. Dispersion curves for the shear waves propagating in the direction of fibers in FCs with $v_f = 0.25$ and (a) $\mu_f/\mu_m = 10$, (b) $\mu_f/\mu_m = 100$, and (c) $\mu_f/\mu_m = 1000$. The FCs are subjected to the uniaxial tension of the magnitude $\lambda = 0.98$ (dashed green curves), $\lambda = 1$ (continuous black curves), $\lambda = 1.5$ (dotted blue curves), and $\lambda = 2$ (dash-dotted red curves). (For interpretation of the references to colour in this figure legend, the reader is referred to the web version of this article.)

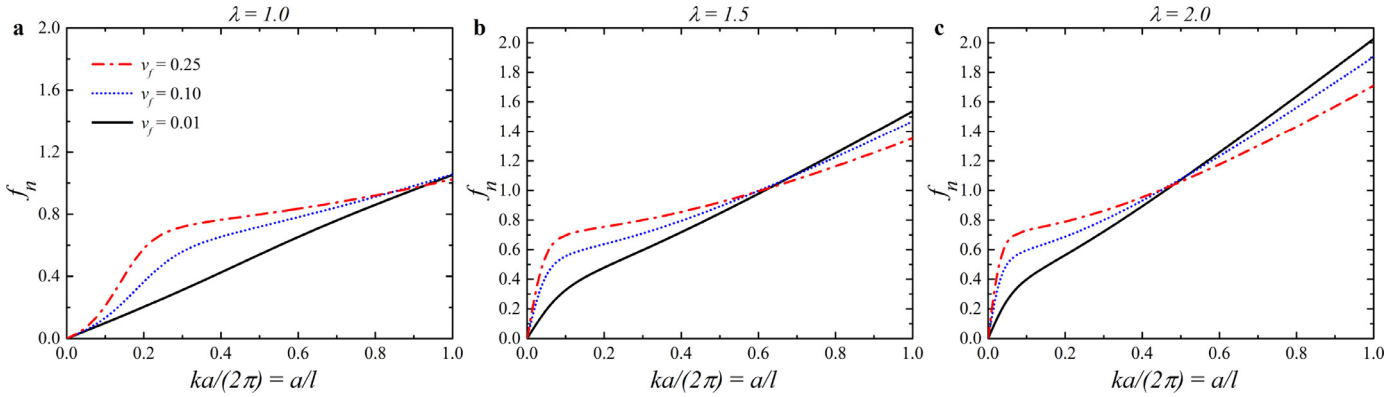


Fig. 3. Dispersion curves for shear waves propagating in the direction of fibers in FCs with $\mu_f/\mu_m = 1000$ in the undeformed state (a) and for the FCs subjected to the uniaxial tension of magnitude $\lambda = 1.5$ (b) and $\lambda = 2$ (c).

and deformed configurations are related via $\mathbf{K}^0 = \mathbf{F}^T \cdot \mathbf{k}$. Here, we present frequencies as functions of wavenumber k in the deformed configuration. Figs. 1–3 correspond to Figs. 7, 8 and 9, respectively, in the original paper (Galich et al., 2017). Thus, the conclusion in Galich et al. (2017) about the weak influence of the applied deformation on short shear waves (with wavelength $l \lesssim 2a$) needs to be corrected. As can be seen from Fig. 2, the applied uniaxial deformation influence shear waves in both long and short wave ranges. All other conclusions in Galich et al. (2017) agree with the dispersion curves presented in Figs. 1–3.

Reference

Galich, P.I., Slesarenko, V., Rudykh, S., 2017. Shear wave propagation in finitely deformed 3D fiber-reinforced composites. Int. J. Solids Struct. 110–111, 294–304.